Neuromethods (2012) 67: 205–218
DOI 10.1007/7657_2011_6

Published online: 25 November 2011

Determination of Cortical Circuit Function Using Current Source-Density Analysis In Vivo

Michael J. Higley

Abstract

The recording of local field potentials (LFPs) has become a major tool in the analysis of electrical signaling in the brain. By yielding information about correlated activity in small neuronal populations, LFPs have been used to study mechanisms of sensory encoding, motor planning, cognitive function, and the occurrence of pathological activity patterns seen in epilepsy. However, the relatively poor spatial resolution of LFP signals often impedes characterization of the cellular processes underlying their generation. Thus, current source-density (CSD) analysis has been developed as a means to enhance the discrimination of extracellular current sinks and sources that are produced by neural synaptic activity. CSD analysis has been used by a number of groups to construct functional maps of the flow of information through cortical networks in vivo. Moreover, the relative technical ease of acquiring data for CSD computation has made this an attractive approach for neuroscientists in a diverse array of fields. Here, we describe the basic theory underlying CSD analysis and give a methodological overview of its application in the rodent neocortex.

Key words: Current source-density, Local field potential, Electrophysiology, In vivo, Laminar, Cortex, Silicon probe

1. Introduction

Brain function is subserved by the electrical signaling properties of individual neurons that receive and integrate analog inputs in the form of synaptic potentials and generate output in the form of action potentials. A basic experimental goal in neuroscience research is to record this electrical activity, both to understand its relationship to behavior and cognition and also to elucidate the cellular mechanisms underlying its generation.

One of the oldest approaches used to characterize neuronal activity is the recording of extracellular field potentials, first described in 1875 by Richard Caton (1). Field potentials are signals generated by the synchronous changes in current flowing across the membranes of individual or groups of neurons, and therefore, through the extracellular space. Events contributing to these potentials include fast sodium action potentials, synaptic

activity, dendritic calcium "spikes" in neuronal dendrites, and large voltage-dependent intrinsic oscillations in single neurons (2, 3). The signals recorded can take a variety of forms, including fast impulses recorded in peripheral nerves, event-related potentials in localized brain regions, and the complex patterns of the electroencephalogram (EEG) spanning the cortical mantle (2, 3).

In particular, the lower frequency (<100 Hz) signals recorded by microelectrodes either inserted into the brain or positioned at the surface, termed local field potentials (LFPs), have been of great interest. LFPs are thought to reflect the linearly summed postsynaptic potentials from neighboring groups of neurons (2–4), and therefore provide an estimation of activity across local populations. Traditionally, LFPs have been used to characterize the spontaneous oscillatory activity of the brain in both healthy conditions and during pathological states such as seizures (2). However, an increasing number of studies have used LFPs to investigate the cellular mechanisms of sensory encoding, motor planning, memory, and decision-making (5–11). In addition, the population activity measured by LFPs appears to be related to the BOLD response measured by fMRI (12), providing a cellular correlate for imaging studies. LFPs have also emerged as a candidate signal for the design and control of neural prostheses (13).

One challenge to the interpretation of LFP data is the relatively poor spatial resolution inherent in these signals. Volume conduction of extracellular potentials through the brain parenchyma significantly impairs determination of the site of origin for LFPs. One solution has been to perform current source-density (CSD) analysis. This approach employs the recording of voltage gradients through geometrically arranged arrays of microelectrodes to estimate extracellular current flow in and out of a proscribed volume of tissue. In this chapter, we briefly review the interpretation of LFP data and the computation of the CSD. We also illustrate some uses of CSD analysis and provide an experimental outline for pursuing this approach in the rodent cortex.

1.1. Origin and Interpretation of Local Field Potentials

Neuronal activity involves current flow across a lipid bilayer membrane, resulting in a potential difference between the intracellular and extracellular spaces. In most cases, this membrane potential is nonuniformly polarized (e.g., the local depolarization of a region of axon produced by a propagating action potential or the depolarization of the dendritic arbor relative to the cell body following synaptic excitation). These potential gradients produce current flow from one part of the cell to another, necessarily generating equal extracellular currents flowing in the opposite direction. At points where net current is directed inward across the membrane, the location is termed a *sink*. Where current is net outward, the location is termed a *source*. The flow of current through the finite conductivity of the extracellular fluid establishes potential

gradients that can be recorded by local electrodes. Thus, LFPs are potentials between two points in extracellular space rather than across a membrane.

Determination of the exact generators of extracellular current flow underlying the LFP is still an area of active research (2). However, in most situations, excitatory synaptic activity mediated by glutamatergic receptors is thought to be the most significant contributor (2, 3). Although fast sodium action potentials generate large transmembrane currents that can be recorded as extracellular potentials, their short duration (~1 ms) limits temporal summation. Furthermore, the low-pass filtering characteristics of the extracellular space attenuate spatial summation of higher frequency events (2). Inhibitory currents through $GABA_A$ receptors may also play a role in the generation of LFPs, particular during highly synchronous activation of GABAergic interneurons (14). However, their contribution is believed to be small because the chloride reversal potential is close to the resting membrane potential. Nevertheless, strong perisomatic shunting inhibition may enhance dendritic inward currents by preventing membrane depolarization and the resulting reduction in excitatory driving force.

Thus, the *magnitude* of the LFP is determined by the total amount of current flowing in or out of a small volume of brain tissue. Consequently, the *time course* of the LFP will closely follow the kinetics of current flow rather than changes in the membrane potential per se. In fact, for brief events shorter than the time constant of the cell (~10–20 ms), transmembrane current is largely due to capacitative charging and is proportional to the first derivative of membrane potential.

To consider an example, we can imagine a glutamatergic synaptic conductance being opened in the apical dendrite of a cortical pyramidal neuron (Fig. 1). We refer to the site of the synapse as an "active" sink because it is generated by a conductance change. Current flowing into the cell at the synapse is balanced by passive current flow out of the cell at some distance away (a "passive" source). This current loop establishes a potential dipole, measurable by an extracellular recording electrode.

From Fig. 1, we can see that the magnitude of the recorded LFP depends on the placement of the electrode relative to the active sink. Specifically, the magnitude of the signal decreases roughly as $1/r$, where r is the distance between the electrode and the sink (15). Furthermore, as dictated by the superposition principle, the LFP recorded at any one site is proportional to the linear summation of all currents generated in vicinity of the electrode (16). A square millimeter of brain tissue can contain ~10^4 neurons and several orders of magnitude greater numbers of synapses, each of which may be active approximately once per second, producing a churning sea of extracellular current flow. LFP data do not allow the discrimination of weak currents

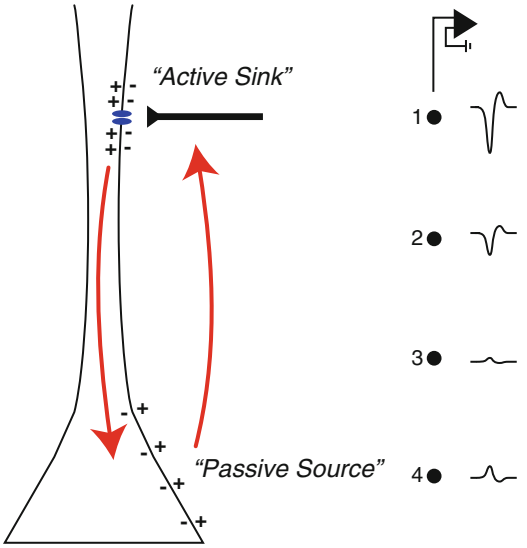

Fig. 1. Schematic illustration of the electrical dipole established by synaptic inputs to the apical dendrite of a cortical pyramidal neuron. Glutamatergic excitation generates an active current sink (inward transmembrane current), while a corresponding passive source (outward transmembrane current) forms at some distance away in the cell body. The direction of current flow is shown by the *curving arrows*. The local field potential (LFP) generated by this synaptic current and recorded by an extracellular electrode varies as a function of distance from the active current sink, as illustrated by the *traces at the right*. Thus, experimental recordings of LFP data have relatively poor spatial resolution and cannot distinguish low amplitude nearby signals from larger more distant signals.

generated by nearby synapses from strong (or highly synchronous) currents generated some distance away. Thus, LFPs give us information that some temporal pattern of synaptic activity has occurred, but the spatial resolution of the underlying current sinks and sources is relatively poor.

1.2. Current Source-Density Analysis

CSD analysis provides a means for enhancing the spatial resolution of current sinks and sources underlying recorded LFPs. Stated directly, the CSD is a scalar quantity that measures the *net* amplitude of extracellular current flowing into and out of neuronal tissue at a given point in space. The additional spatial information is derived from the recording of LFPs at multiple locations and analyzing their spatial distribution. This can be performed by sequentially moving a single microelectrode, but is most often done using a single multisite recording array, allowing simultaneous recording of LFPs over a large volume of tissue.

The utility of CSD analysis is illustrated in Fig. 2 (see Sect. 3 for the computation of the CSD). Here, LFPs were recorded from

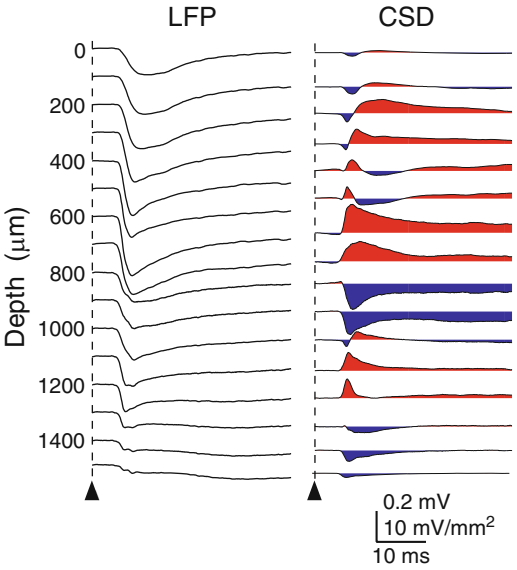

Fig. 2. Example of sensory-evoked LFP data and the corresponding current sinks and sources. The LFPs (*left traces*) were recorded by a 16-channel silicon probe inserted into the barrel cortex of an anesthetized rat. Deflection of a single somatotopically aligned whisker (*black triangle*) produced a complex set of voltage traces at multiple locations throughout the cortical depths. The CSD traces at the *right*, computed using methods described in the text, elucidate the synaptic currents underlying generation of the LFPs. Consistent with known anatomy, whisker deflection evokes an early thalamocortical sink in mid-layers, followed by delayed sinks in superficial and deeper layers. Thus, CSD analysis provides a functional map for the flow of excitation in cortical circuits.

a 16-site silicon-based laminar recording array inserted into the barrel cortex of an anesthetized rat. Recording sites are separated by 100 μm, and the entire probe spans most of the cortical thickness. The barrel cortex is organized in a columnar pattern, with neurons in vertical register being most strongly driven by deflection of the same somatotopically aligned "principal" whisker (6, 17, 18). Here, average LFPs at each site were recorded following deflection of the principal whisker (left traces). Note that the spatial locations of synaptic inputs evoked by whisker deflection are difficult to identify from the LFP data. However, the computed CSD for each site is shown at the right, with positive values (shown in red) representing current sinks and negative values (shown in blue) representing current sources. These traces reveal that whisker deflection produces early excitation (current sink) at a depth of 500–700 μm, corresponding to cortical layer 4. Subsequently, delayed excitation appears in superficial and deeper cortical layers. These data provide a picture of the intracolumnar flow of sensory information and agree with the known anatomy of thalamocortical and intracortical projections (19–21). Thus, the power of CSD analysis is the ability to generate a functional

spatiotemporal map of population synaptic activity in vivo. In this respect, the CSD provides a unique source of information that cannot be gained from traditional intracellular recordings, which measure the integrated synaptic responses at the cell body, or extracellular single unit recordings, which reveal only suprathreshold activity.

CSD analysis has been successfully applied to the analysis of spontaneous and evoked neuronal activity in structures throughout the brain, including the cortex, cerebellum, hippocampus, retina, and brainstem. A thorough discussion of these works is beyond the scope of this chapter. However, to illustrate some of the possible uses of the CSD, three examples are presented here.

First, as shown above, CSD analysis has been used by multiple groups to map the flow of intra- and intercolumnar excitation in somatosensory (6, 7, 18), auditory (5), and visual (22) cortices. In combination with anatomical knowledge, this approach has been particularly valuable in determining the contribution of ascending (thalamocortical) versus horizontal (intracortical) inputs to sensory encoding. In the case of the rat whisker system, Higley and Contreras (6) used computation of the CSD along with pharmacological inactivation of intracortical circuits to show that horizontal inputs from adjacent cortical regions do not contribute significantly to suppressive interactions between sensory stimuli. By contrast, Happel et al. (5) showed that for the primary auditory cortex, long-range horizontal connections terminating in superficial layers are critical to the generation of spectral tuning receptive fields. Similarly, Chen et al. (22) used laminar activation profiles in ventral areas V4 and IT of the macaque visual system to conclude that inputs from dorsal stream pathways and nonspecific thalamic nuclei modulate neuronal activity in these areas.

Second, CSD analysis has been used to determine the functional terminal arborization of a single presynaptic neuron in vivo. In an elegant study, Swadlow et al. (7) recorded the average LFPs triggered in the rat barrel cortex by a simultaneously recorded single unit in the somatotopically aligned somatosensory thalamus. Computation of the underlying active sinks revealed excitatory inputs to layers 4 and 6, precisely matching the anatomical projections of thalamocortical neurons. In a later study, they further showed that this functional map was unaltered by changes in behavioral state, despite changes in overall patterns of cortical activity (23).

Third, CSD analysis has also been used to analyze the anatomical substrates of spontaneously occurring oscillations in the rodent cortex and hippocampus. Kandel and Buzsaki (24) recorded LFPs in the neocortex of both awake and anesthetized rats during natural sleep spindles and epileptiform high-voltage spike-and-wave activity. Comparing the corresponding sinks and sources to those evoked by sensory stimulation, the authors concluded that these spontaneous oscillations are largely mediated by intracortical circuits.

1.3. Derivation of the CSD

We now give a brief overview of the computation of the CSD. The reader is referred to additional resources for a more in depth mathematical treatment of these concepts (3, 16, 25).

The relationship between the transmembrane current, i_m, (e.g., that is produced by synaptic activation) and the concurrent three-dimensional extracellular field potential, Φ, is given by:

$$i_m = K \times \left[\frac{\partial^2 \Phi}{\partial x^2} + \frac{\partial^2 \Phi}{\partial y^2} + \frac{\partial^2 \Phi}{\partial z^2}\right]$$

where K is a proportionality constant that includes the conductivity of the extracellular fluid. A practical difficulty in applying this relationship is the necessity of measuring the LFP in three orthogonal axes.

However, if the volume of tissue being analyzed is laminar, consisting of stacked two-dimensional planes of uniform anatomy, we can assume that the change in potential within each of these planes is zero, and therefore:

$$\frac{\partial^2 \Phi}{\partial x^2} = \frac{\partial^2 \Phi}{\partial y^2} = 0$$

and the extracellular current is directly proportional to the second spatial derivative of the LFPs recorded along the axis perpendicular to the laminar structure.

In the case of the neocortex (and possibly the hippocampus and cerebellum), there is reason to believe this assumption is justified. Cortical laminae comprise multiple cell-body and dendritic layers, each with approximately uniform synaptic inputs. Furthermore, the neocortex is typically arranged as a columnar structure, with intracolumnar diameters of several hundred microns (26). Recent studies have suggested that >95% of the LFP signal originates within 250 μm of the recording site, suggesting that most currents are generated by synapses in the same column and exhibit similar patterns of spontaneous and evoked activity (27, 28). Thus, assuming a uniform laminar signal under these conditions is reasonable. Nevertheless, in their studies of the cerebellum, Nicholson and Llinas (29) recommended a full three-dimensional analysis using multiple arrays of electrodes arranged in a three-dimensional configuration. Furthermore, Pettersen et al. (30) developed an alternative analysis, termed inverse CSD (iCSD), where laminar heterogeneity and differential spatial distribution of conductivity are explicitly considered and which may yield more accurate calculations under some circumstances.

In the simplified case, LFP measurements are taken from a finite number of sampling points (e.g., the 16 channels of a silicon-based laminar probe). From these discrete points, the second spatial derivative can be calculated using any one of

standard difference formulas. We have adopted the following procedure from Freeman and Nicholson (25).

Take LFP measurements at three neighboring points, V_0, V_a, and V_b, such that:

$$V_0 = V(z, t)$$

$$V_a = V(z - 2\Delta z, t)$$

$$V_b = V(z + 2\Delta z, t),$$

where z is the location along the recording axis and Δz is the spacing between consecutive recording sites. A simple approximation of the second spatial derivative, discussed by Freeman and Nicholson (25), is given by:

$$\frac{\partial^2 V(t)}{\partial z^2} = i_m(t) \approx \frac{V_b + V_a - 2V_0}{(2\Delta z)^2}$$

Here, $i_m(t)$ is called the current source-density function.

A number of other more complicated estimations for the second spatial derivative are possible. However, a direct comparison of the computed CSD values for several cases did not find a considerable improvement in the accuracy of the calculation (25).

It may also be apparent that, if n separate LFP channels are recorded, only n-4 are available for the CSD computation, reducing the area over which the CSD can be derived. However, we and other authors have taken advantage of the observation that, in many cases, the recorded potentials do not vary significantly above and below the first and last recording site, respectively. In this situation, Vaknin et al. (31) showed that extrapolating the LFP data at the two extremes produced an accurate calculation of the underlying CSD, and this procedure was used to generate the CSD traces from the corresponding LFP data in Fig. 2.

2. Materials

2.1. Surgical Equipment

- Experimental animals (rats)
- Stereotaxic frame with anesthesia head holder and arms for electrode holders (Model#930, #1460, #1929-B, David Kopf, Inc.).
- Heating blanket
- Surgical tools (forceps, scissors, scalpel, etc.)
- High-speed dental drill
- Sterile saline
- Anesthetic (Isoflurane)

- Local anesthetic (Lidocaine 1%)
- Surgical scrub (Betadine)
- Hair trimmer
- Dental acrylic

2.2. Electrophysiological Recordings

- 16-channel silicon-based laminar probe with A-type connector (Part# A1×16-3mm100-413, Neuronexus Technologies, Inc.)
- Connecting cable (28 ga insulated wire)
- Silver wire (~32 ga)
- Two 8-channel differential amplifiers (Model HiZ×8, FHC, Inc.), custom built with low cutoff filter settings of 0.1 or 1.0 Hz for LFP recordings

2.3. Data Acquisition and Analysis

- Power1401 Acquisition System (Cambridge Electronic Design, Inc.)
- Spike2 acquisition software (Cambridge Electronic Design, Inc.)
- Standard computer (highest processing power available is recommended)
- IgorPro (Wavemetrics, Inc.)
- DataAccess (Bruxton, Inc.)

3. Methods

3.1. Hardware

In order to record LFP data at multiple sites through the cortical depth, the 16-channel silicon-based laminar recording array from Neuronexus Technologies provides a high quality signal in a compact and economical form factor (Fig. 3). Each recording site is equally spaced at 100 μm intervals, which is sufficient to span the rat somatosensory cortex. The size of the recording site can be specified at either 177 or 413 or 703 μm^2. For recording LFPs, we recommend either of the larger-sized probes. Thus, the appropriate part number is A1×16-3mm100-413.

A variety of printed circuit board connectors ("Probe Packages") are also available. For acute recordings, we recommend the A16 version. This connector consists of a standard 2 × 8 dual-inline-pin (DIP) block, with a pin length of 5.5 mm and pin spacing of 2.5 mm. Cables can be directly soldered to these pins, or matching connectors can be obtained from any small electronics dealer.

An amplifier with sufficient channels is also required. We have successfully used two 8-channel HiZ×8 differential amplifiers from FHC, Inc. However, note that the standard low cutoff filter

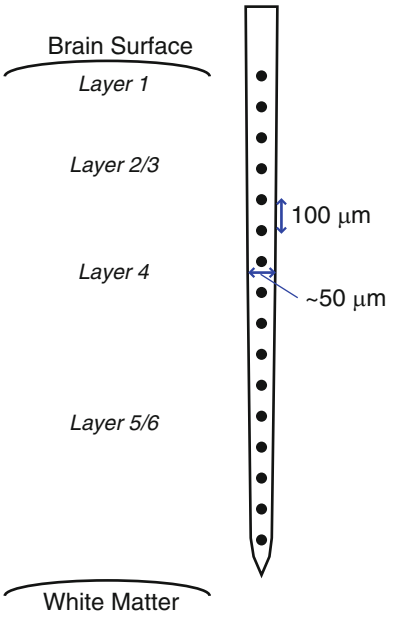

Fig. 3. Schematic illustration of the 16-channel silicon probe, available from Neuronexus, Inc., typically used to record LFP data in laminar structures, to be used for subsequent computation of the CSD. The probe is suitable for spanning the depth of the rat neocortex.

settings (100–500 Hz) are insufficient for LFP data. It is necessary to request a custom circuit with a low cutoff of 0.1 or 1 Hz. The headstage consists of eight pairs of pin inputs for multiple bipolar recordings. In this case, each recording site from the probe is directed to an individual positive terminal and a ganged reference signal (see below) is directed to each negative terminal (Fig. 4).

3.2. Data Acquisition

For recording LFP data, a sampling rate of 10 kHz is sufficient (if you wish to simultaneously record multiunit activity from the probe recording sites, this rate should be >20 kHz). Recording 16 channels at this rate requires considerable bandwidth for data acquisition. The Power1401 from Cambridge Electronic Design (Cambridge, UK) is a data acquisition board that is suitable for these recordings, and allows, in different configurations, up to 64 channels of waveform data acquisition. The Power 1401 requires the use of Spike2 software, also from Cambridge Electronic Design.

3.3. Analysis

Spike2 saves acquired data in a proprietary format. Although some analysis is possible with Spike2, the increased flexibility of dedicated analysis software warrants exporting the raw data. We highly recommend IgorPro from Wavemetrics as an easy-to-learn and flexible environment for waveform data analysis.

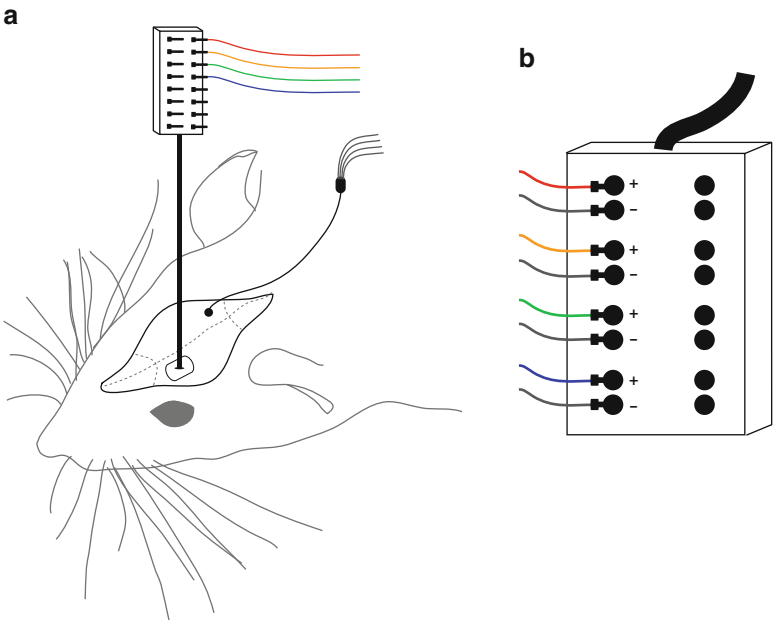

Fig. 4. Schematic illustration of the recording setup used to obtain LFP and CSD data from the rat cortex. The probe is inserted into the cortex of an anesthetized rat, positioned normal to the brain surface. Each channel of the probe is connected to an individual positive terminal on the headstage of a differential amplifier (Only four wires are shown in the diagram). Reference signals are provided by a silver wire, inserted between the dura and the inner skull surface and connected to a cable bus directed to the negative terminals of the headstage.

To export data from Spike2 to IgorPro, we recommend DataAccess by Bruxton. This software adds several user-accessible routines to IgorPro, allowing the importing of Spike2 files. Alternatively, DataAccess has a simple graphical interface for managing data conversion.

Once the data has been moved to IgorPro, standard analysis methods can be used to generate averaged LFP traces around selected time-points. From these averages, the CSD can be computed algebraically as detailed in the previous section.

3.4. Surgical Setup

The experimental approach described briefly here is performed under isoflurane anesthesia. The reader is referred to other excellent chapters in the present volume by Cardin, Crochet, and Vyazovskiy et al. for additional detailed information on surgical protocols.

3.5. Electrode Placement

1. Induce anesthesia and position the rat into the stereotaxic apparatus. During initial surgical manipulations, isoflurane should be set to ~2%. After incisions and craniotomy have been completed and the animal's depth of anesthesia stabilizes, isoflurane can be reduced to ~0.5%.

2. Expose the skull, and make a small rectangular craniotomy over the appropriate recording site (~200–300 μm per side). The craniotomy should be large enough to accommodate positioning the electrode but no larger. The detached piece of bone can be removed with forceps, exposing the dura. Flushing with sterile saline will remove any accumulated blood. It may take 2–3 min for small severed vessels to coagulate.
3. At this point, the grounding wire should be placed. This is typically done be making a small burr hole through the skull at some distance (>2 mm) from the recording site. Insert a thin, chlorided silver wire through the burr hole to rest between the dura and interior skull surface. Silver wire can be readily chlorided by soaking in bleach for 1–2 h, followed by rinsing with water. Use of poorly chlorided reference electrodes may generate a large voltage drop that may saturate the amplifier headstage. The exterior end of the wire should be connected to a ganged grounding bus, consisting of 16 individual wires that will serve as the references for each recording channel (Fig. 3). This silver wire can be held in place on the skull surface by application of a small amount of dental acrylic.
4. Using a fine syringe tip (30 ga) or fine dissecting scissors, make a small incision in the dura to allow electrode penetration.
5. When handling the probe, only touch the printed circuit board. Position the probe in the stereotaxic manipulator and attach the connector to the headstage. This will minimize post-implant movement. Using the manipulator, orient the probe so that its principal axis is normal to the brain surface. Gradually lower the probe into the brain. If buckling occurs, wait for the probe to work its way into the tissue (may take several minutes). Continue lowering the probe until the dorsal-most recording site is even with the brain surface.
6. Electrode insertion often results in temporary spreading depression, where neural activity around the electrode is silenced for a period of time. Thus, it is recommended to wait for ~30 min following electrode placement to begin recordings.
7. Probes can be reused for multiple experiments if rinsed gently with hydrogen peroxide or enzymatic contact lens cleaner followed by distilled water at the conclusion of the recording session.

References

1. Caton R (1875) The electrical currents of the brain. Br Med J 2:278
2. Ebersole JS, Pedley TA (eds) (2003) Current practice of clinical electroencephalography. Lippincott Williams & Wilkins, Philadelphia
3. Mitzdorf U (1985) Current source-density method and application in cat cerebral cortex: investigation of evoked potentials and EEG phenomena. Physiol Rev 65:37–100
4. Buzsaki G (2004) Large-scale recording of neuronal ensembles. Nat Neurosci 7:446–451
5. Happel MF, Jeschke M, Ohl FW (2010) Spectral integration in primary auditory cortex attributable to temporally precise convergence of thalamocortical and intracortical input. J Neurosci 30:11114–11127
6. Higley MJ, Contreras D (2007) Cellular mechanisms of suppressive interactions between somatosensory responses in vivo. J Neurophysiol 97:647–658
7. Swadlow HA, Gusev AG, Bezdudnaya T (2002) Activation of a cortical column by a thalamocortical impulse. J Neurosci 22:7766–7773
8. Henrie JA, Shapley R (2005) LFP power spectra in V1 cortex: the graded effect of stimulus contrast. J Neurophysiol 94:479–490
9. Kreiman G, Hung CP, Kraskov A et al (2006) Object selectivity of local field potentials and spikes in the macaque inferior temporal cortex. Neuron 49:433–445
10. Pesaran B, Pezaris JS, Sahani M et al (2002) Temporal structure in neuronal activity during working memory in macaque parietal cortex. Nat Neurosci 5:805–811
11. Scherberger H, Jarvis MR, Andersen RA (2005) Cortical local field potential encodes movement intentions in the posterior parietal cortex. Neuron 46:347–354
12. Logothetis NK, Pauls J, Augath M et al (2001) Neurophysiological investigation of the basis of the fMRI signal. Nature 412:150–157
13. Andersen RA, Musallam S, Pesaran B (2004) Selecting the signals for a brain-machine interface. Curr Opin Neurobiol 14:720–726
14. Ylinen A, Bragin A, Nadasdy Z et al (1995) Sharp wave-associated high-frequency oscillation (200 Hz) in the intact hippocampus: network and intracellular mechanisms. J Neurosci 15:30–46
15. Bedard C, Kroger H, Destexhe A (2006) Model of low-pass filtering of local field potentials in brain tissue. Phys Rev E Stat Nonlin Soft Matter Phys 73:051911
16. Johnston D, Wu SM (1997) Foundations of cellular neurophysiology. MIT Press, Cambridge
17. Simons DJ, Woolsey TA (1979) Functional organization in mouse barrel cortex. Brain Res 165:327–332
18. Di S, Baumgartner C, Barth DS (1990) Laminar analysis of extracellular field potentials in rat vibrissa/barrel cortex. J Neurophysiol 63:832–840
19. Bernardo KL, Woolsey TA (1987) Axonal trajectories between mouse somatosensory thalamus and cortex. J Comp Neurol 258: 542–564
20. Lubke J, Roth A, Feldmeyer D et al (2003) Morphometric analysis of the columnar innervation domain of neurons connecting layer 4 and layer 2/3 of juvenile rat barrel cortex. Cereb Cortex 13:1051–1063
21. Shepherd GM, Svoboda K (2005) Laminar and columnar organization of ascending excitatory projections to layer 2/3 pyramidal neurons in rat barrel cortex. J Neurosci 25:5670–5679
22. Chen CM, Lakatos P, Shah AS et al (2007) Functional anatomy and interaction of fast and slow visual pathways in macaque monkeys. Cereb Cortex 17:1561–1569
23. Stoelzel CR, Bereshpolova Y, Swadlow HA (2009) Stability of thalamocortical synaptic transmission across awake brain states. J Neurosci 29:6851–6859
24. Kandel A, Buzsaki G (1997) Cellular-synaptic generation of sleep spindles, spike-and-wave discharges, and evoked thalamocortical responses in the neocortex of the rat. J Neurosci 17:6783–6797
25. Freeman JA, Nicholson C (1975) Experimental optimization of current source-density technique for anuran cerebellum. J Neurophysiol 38:369–382
26. Mountcastle VB (1998) The cerebral cortex. Harvard University Press, Cambridge
27. Katzner S, Nauhaus I, Benucci A et al (2009) Local origin of field potentials in visual cortex. Neuron 61:35–41
28. Xing D, Yeh CI, Shapley RM (2009) Spatial spread of the local field potential and its laminar variation in visual cortex. J Neurosci 29:11540–11549

29. Nicholson C, Llinas R (1975) Real time current source-density analysis using multi-electrode array in cat cerebellum. Brain Res 100:418–424
30. Pettersen KH, Devor A, Ulbert I et al (2006) Current-source density estimation based on inversion of electrostatic forward solution: effects of finite extent of neuronal activity and conductivity discontinuities. J Neurosci Methods 154:116–133
31. Vaknin G, DiScenna PG, Teyler TJ (1988) A method for calculating current source density (CSD) analysis without resorting to recording sites outside the sampling volume. J Neurosci Methods 24:131–135